J. Fluid Mech. (1999), *vol.* 401, *pp.* 311–338. Printed in the United Kingdom

Linear stability of pathological detonations

By GARY J. SHARPE

Department of Applied Mathematics, University of Leeds, Leeds LS2 9JT, UK

(Received 11 November 1998 and in revised form 5 August 1999)

In this paper we investigate the linear stability of detonations in which the underlying steady one-dimensional solutions are of the pathological type. Such detonations travel at a minimum speed, which is greater than the Chapman–Jouguet (CJ) speed, have an internal frozen sonic point at which the thermicity vanishes, and the unsupported wave is supersonic (i.e. weak) after the sonic point. Pathological detonations are possible when there are endothermic or dissipative effects present in the system. We consider a system with two consecutive irreversible reactions A→B→C, with an Arrhenius form of the reaction rates and the second reaction endothermic. We determine analytical asymptotic solutions valid near the sonic pathological point for both the one-dimensional steady equations and the equations for linearized perturbations. These are used as initial conditions for integrating the equations. We show that, apart from the existence of stable modes, the linear stability of the pathological detonation is qualitatively the same as for CJ detonations for both one- and two-dimensional disturbances. We also consider the stability of overdriven detonations for the system. We show that the frequency of oscillation for one-dimensional disturbances, and the cell size based on the wavenumber with the highest group velocity for two-dimensional disturbances, are both very sensitive to the detonation speed for overdriven detonations near the pathological speed. This dependence on the degree of overdrive is quite different from that obtained when the unsupported detonation is of the CJ type.

1. Introduction

A detonation is a supersonic (with respect to the unburnt fuel) regime of burning in which a strong shock ignites the fuel, which then burns to equilibrium behind the shock, and the energy thereby released helps to drive the shock.

The governing equations for such a process admit steady (in the frame of the shock), one-dimensional solutions, the so-called Zeldovich–Neumann–Döring waves (e.g. von Neumann 1942). Wood & Salsburg (1960) considered the possible steady one-dimensional flows for a very general system with an arbitrary number of reversible reactions. They showed that there were three types of steady, one-dimensional detonation wave. The detonation with the minimum possible speed corresponds to the Chapman–Jouguet (CJ) detonation, where the flow is equilibrium sonic at the end of the reaction zone. However, they showed that the CJ detonation might not occur, but that instead a pathological detonation exists which travels at a speed which is greater than or equal to the CJ speed. For such pathological detonations the reaction zone has an internal frozen sonic point at which the thermicity vanishes and the detonation has two possible wave structures downstream of the sonic point, supersonic or subsonic, corresponding to unsupported and supported pathological detonations respectively. Overdriven detonations, with detonations speeds greater than the minimum possible speed are subsonic throughout and correspond to piston supported detonations.

However, experiments (Fickett & Davis 1979; Lee 1984) reveal that detonation fronts usually have a complicated three-dimensional, time-dependent structure with interior transverse waves. Galloping detonations in which the front oscillates longitudinally occur when blunt bodies move through a reactive gas at near CJ velocities. In round tubes spinning detonations are observed in which the transverse waves rotate about the tube axis. Perhaps of most interest are the cellular detonations that appear in rectangular tubes. If the tube width is not very much larger than the natural cell size the detonation can create remarkably regular diamond shaped patterns in soot deposited on the walls of the tubes. In these cases the steady one-dimensional waves are unstable to perturbations in the flow.

A first step in understanding such instabilities is a linear stability analysis of the underlying steady wave. Such an analysis was pioneered by Erpenbeck (1962), who developed a method which determined the overall stability of a detonation for a given set of parameters using Laplace transforms. Normal mode approaches to the linear stability problem were developed by Lee & Stewart (1990) and Sharpe (1997*a*). In the method of Sharpe (1997*a*) asymptotic solutions are found near singularities in the linearized equations which are used as initial conditions for integrating these equations towards the shock. This was found to be a more efficient method than that of Lee & Stewart (1990) who integrated the linearized equations from the shock into the reaction zone.

Most of the work on the linear stability analysis of detonations has been concerned with an idealized system with one, irreversible reaction with an Arrhenius form of the reaction rate (Short & Stewart 1997, 1998, 1999; Sharpe 1997*a*, *b*; Short 1996*a*, *b*, 1997; Lee & Stewart 1990; Erpenbeck 1964, 1966). One-dimensional, time-dependent numerical simulations (Sharpe & Falle 1998; Williams, Bauwens & Oran 1996; Bourlioux, Majda & Roytburd 1991; Fickett & Wood 1966) show that the linear stability analyses give excellent predictions of the frequencies and neutral stability values near the stability boundaries, and have led to the linear stability analyses being used as benchmarks for testing such codes. Unfortunately no rigorous comparison between the multi-dimensional linear stability results and time-dependent calculations have been performed due to the prohibitively high resolution required for such numerical simulations.

Pathological detonations are not possible for such idealized single irreversible reaction detonations. However, more complicated systems (e.g. those with endothermic stages of the reaction, mole changes during the reaction, more than one reversible reaction, transport effects, relaxational degrees of freedom, curvature of the detonation front; see Fickett & Davis 1979 for examples) allow the pathological type of steady detonation to be possible and thus forbid the CJ type. There has been some work on the linear stability of more complicated detonations. Short & Quirk (1997) carried out a linear stability analysis and one-dimensional numerical simulations of a three-step chain-branching reaction. However, they set the heat absorption of an endothermic stage of the reaction to zero so that the steady detonation is of a CJ type. If this heat of reaction is not zero then pathological detonations may occur. Kriminski, Bychkov & Liberman (1998) calculated the one-dimensional linear stability of nuclear detonations in white dwarf stars, which are believed to be responsible for Type Ia Supernovae events. They used only a single reaction, representing the very early stages of the burning, so that the steady detonation was again of the CJ type. However, it is known that if the full nuclear reaction network is used then the detonation is actually of the pathological type (Wiggins, Sharpe & Falle 1998; Khokhlov 1989). It is therefore important to perform a linear stability analysis of a steady pathological detonation to see if, and how, this differs from the stability of CJ detonations.

The plan of the paper is as follows: § 2 gives the governing equations of the system, together with the non-dimensional variables; the steady one-dimensional solutions of these equations are considered in § 3; the linearized equations are determined in § 4; the method for determining the eigenvalues is described in § 5; the results are presented in § 6 (for one-dimensional disturbances) and § 7 (for multi-dimensional disturbances); § 8 contains the conclusions.

2. Governing equations

In this paper we use a model system with two consecutive irreversible reactions A→B→C, with Arrhenius forms of the reaction rates and the second reaction endothermic. The governing equations are

$$\left.\begin{gathered}\frac{\mathrm{D}\rho}{\mathrm{D}t}+\rho\nabla\cdot\boldsymbol{v}=0,\quad \rho\frac{\mathrm{D}\boldsymbol{v}}{\mathrm{D}t}=-\nabla p,\quad \frac{\mathrm{D}e}{\mathrm{D}t}+p\frac{\mathrm{D}\rho^{-1}}{\mathrm{D}t}=0,\\ \frac{\mathrm{D}\lambda_1}{\mathrm{D}t}=\frac{W_1}{\rho},\quad \frac{\mathrm{D}\lambda_2}{\mathrm{D}t}=\frac{W_2}{\rho},\quad \frac{\mathrm{D}}{\mathrm{D}t}=\frac{\partial}{\partial t}+\boldsymbol{v}\cdot\nabla,\end{gathered}\right\} \tag{2.1}$$

where $\boldsymbol{v}=(u,v,w)$ is the fluid velocity in the laboratory frame, ρ the density, p the pressure, e the internal energy per unit mass, λ_i the reaction progress variable of the ith reaction ($i=1$ or 2, with $\lambda_i=1$ for unburnt and $\lambda_i=0$ for burnt), γ the (constant) ratio of specific heats and W_i the reaction rate of the ith reaction. The internal energy per unit mass is given by

$$e(\rho,p,\lambda)=\frac{p}{(\gamma-1)\rho}-Q,$$

where

$$Q=q_1(1-\lambda_1)+q_2(1-\lambda_2)$$

is the total heat release and q_i is the constant heat of reaction for the ith reaction. Note that $q_2<0$ since the second reaction is assumed to be endothermic. The mass fractions x_A, x_B, x_C of species A, B, C are related to the reaction progress variables by

$$\mathrm{x}_A=\lambda_1,\quad \mathrm{x}_B=\lambda_2-\lambda_1,\quad \mathrm{x}_C=1-\lambda_2.$$

We assume an Arrhenius form of the reaction rates and a perfect gas:

$$W_1=-K_1\rho\lambda_1\mathrm{e}^{(-T_{A1}/T)},\quad W_2=K_2\rho(\lambda_1-\lambda_2)\mathrm{e}^{(-T_{A2}/T)},\quad T=\frac{\mu p}{R\rho},\quad c^2=\frac{\gamma p}{\rho},$$

where T is the temperature, c the sound speed, T_{Ai} the activation temperature of the ith reaction, K_i the constant rate coefficient for the ith reaction, R the universal gas constant and μ the (constant) mean molecular weight. It is also useful to define the sonic parameter

$$\eta=c^2-u^2.$$

The shock (Rankine–Hugoniot) conditions are

$$\left.\begin{gathered}[\rho(\boldsymbol{D}-\boldsymbol{v})\cdot\boldsymbol{n}]_+=[\rho(\boldsymbol{D}-\boldsymbol{v})\cdot\boldsymbol{n}]_-=m,\quad p_+-p_-=m^2\left(\frac{1}{\rho_-}-\frac{1}{\rho_+}\right),\\ \left[e+\frac{p}{\rho}+\tfrac{1}{2}|\boldsymbol{D}-\boldsymbol{v}|^2\right]_+=\left[e+\frac{p}{\rho}+\tfrac{1}{2}|\boldsymbol{D}-\boldsymbol{v}|^2\right]_-,\quad \boldsymbol{v}_+\cdot\boldsymbol{t}=\boldsymbol{v}_-\cdot\boldsymbol{t},\quad \lambda_{i+}=1,\end{gathered}\right\} \tag{2.2}$$

where $\boldsymbol{D}$ is the normal shock velocity measured in the laboratory frame, $\boldsymbol{n}$ is the unit

normal to the shock and $\boldsymbol{t}$ any tangent vector, with the +,− subscripts referring to states immediately behind and ahead of the shock respectively.

Henceforth we use a bar ($^-$) to denote dimensional quantities, a zero (0) subscript to denote steady, unperturbed quantities, an s superscript to denote quantities at a sonic point, a p superscript to denote quantities at the pathological point and an infinity (∞) superscript to denote quantities at the end of the reaction zone.

We non-dimensionalize by putting

$$\left.\begin{gathered}\rho = \frac{\bar{\rho}}{\bar{\rho}_-}, \quad \boldsymbol{v} = \frac{\bar{\boldsymbol{v}}}{\bar{D}}, \quad p = \frac{\bar{p}}{\bar{\rho}_-\bar{D}^2}, \quad T = \frac{p}{\rho} = \frac{\bar{R}\bar{T}}{\bar{\mu}\bar{D}^2}, \quad t = \frac{\bar{K}_1\bar{t}}{\alpha_1}, \quad \boldsymbol{r} = \frac{\bar{K}_1\bar{\boldsymbol{r}}}{\alpha_1\bar{D}}, \\ q_1 = \frac{\bar{q}_1}{\bar{D}^2}, \quad q_2 = \frac{\bar{q}_2}{\bar{D}^2},\end{gathered}\right\} \tag{2.3}$$

where $\bar{D}$ is the speed of the steady detonation wave, $\boldsymbol{r} = (x, y, z)$ is the position vector and α_1 is a scale factor chosen so that the characteristic length scale is the half-reaction length of the first reaction, i.e. the distance between the shock and the point at which $\lambda_1 = 1/2$. We then define non-dimensional activation temperatures, τ_1, τ_2, by

$$\tau_1 = \frac{\bar{R}\bar{T}_{A1}}{\bar{\mu}\bar{D}^2}, \quad \tau_2 = \frac{\bar{R}\bar{T}_{A2}}{\bar{\mu}\bar{D}^2},$$

and the non-dimensional pressure in the ambient material by

$$p_- = \frac{\bar{p}_-}{\bar{\rho}_-\bar{D}^2}.$$

In terms of these non-dimensional variables equations (2.1) are unchanged in form except that the reaction rates are now given by

$$W_1 = -\alpha_1\rho\lambda_1 \exp(-\tau_1\rho/p), \quad W_2 = \alpha_2\rho(\lambda_1 - \lambda_2)\exp(-\tau_2\rho/p),$$

where $\alpha_2 = \alpha_1\bar{K}_2/\bar{K}_1$. Let $\alpha = \alpha_2/\alpha_1$.

The majority of the results of previous work on the linear stability of detonations have been given in terms of the more familiar scalings of Erpenbeck (1964), who scaled the activation temperature and heat of reaction by the temperature in the ambient material. In terms of this scaling we define

$$E_1 = \frac{\bar{T}_{A1}}{\bar{T}_-}, \quad E_2 = \frac{\bar{T}_{A2}}{\bar{T}_-}, \quad Q_1 = \frac{\bar{q}_1\bar{\mu}}{\bar{R}\bar{T}_-}, \quad Q_2 = \frac{\bar{q}_2\bar{\mu}}{\bar{R}\bar{T}_-}.$$

Note that

$$\bar{T}_- = \frac{\bar{\mu}\bar{p}_-}{\bar{R}\bar{\rho}_-} = \frac{\bar{\mu}}{\bar{R}}\bar{D}^2 p_-$$

so that the conversion between his scalings and ours is given by

$$E_i = \frac{\tau_i}{p_-}, \quad Q_i = \frac{q_i}{p_-}.$$

Throughout this paper we set

$$\gamma = 1.2, \quad \alpha = 1,$$

and, unless otherwise specified,

$$Q_1 = 100, \quad Q_2 = -75.$$

Note that for $\alpha = 1$ and $\tau_1 = \tau_2 = 0$ this reduces to the pathological detonation model of Fickett & Davis (1979).

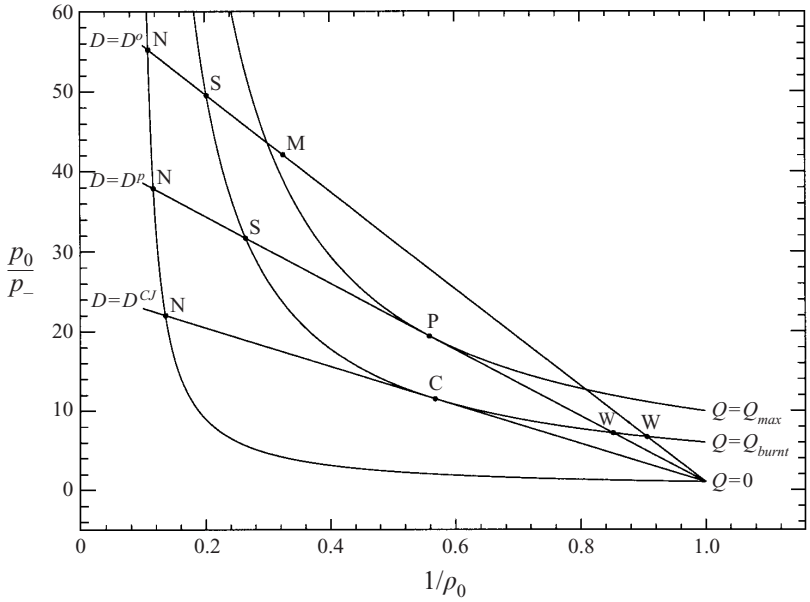

FIGURE 1. Hugoniot curves and Rayleigh lines in the $(1/\rho_0, p_0)$-plane for $Q_1 = 100$, $Q_2 = -75$, $\alpha = 1$, $\gamma = 1.2$.

3. The steady one-dimensional solution

3.1. *Qualitative behaviour of the steady solution*

The properties of the steady detonation wave can be understood by considering the Hugoniot curves and Rayleigh lines (see, for example, Fickett & Davis 1979) in a $(p_0, 1/\rho_0)$-plane (figure 1). For a given value of the detonation speed the steady solution is confined to a Rayleigh line, which represents conservation of mass and momentum. The Hugoniot curves represent conservation of energy for fixed values of the reaction progress variables (or equivalently in this case for a given value of the total heat release). Note that the Hugoniot curve is a projection onto the plane of a curve in the space of the chemical and thermodynamic variables. Since the second reaction is endothermic there can be a maximum in the heat release within the detonation wave, in which case there are two points within the wave which have the same value of the heat release.

The steady solution evolves along the Rayleigh line, crossing each of the Hugoniot curves in turn until the equilibrium (i.e. burnt) state is reached (i.e. the Hugoniot curve corresponding to $Q = Q_{burnt}$ in figure 1). An important point is that whenever a Rayleigh line and Hugoniot curve are tangent to each other the flow is sonic at the tangent point, and is subsonic above that point and supersonic below it (Landau & Lifshitz 1959).

The shock takes the state to the Neumann point N, where the Rayleigh line and the (unburnt) Hugoniot curve corresponding to $Q = 0$ cross. The Chapman–Jouguet condition is that the flow is sonic at the end of the reaction zone, i.e the CJ detonation speed corresponds to the Rayleigh line which is tangent to the complete reaction Hugoniot curve (the line corresponding to $D = D^{CJ}$ in figure 1). For detonation speeds below this value there can be no steady solution since the corresponding Rayleigh line does not touch the complete reaction Hugoniot curve and so the equilibrium state cannot be reached. However, when the detonation has an endothermic stage

the complete reaction Hugoniot curve may also be a Hugoniot curve for incomplete reaction. Then other incomplete reaction Hugoniot curves, corresponding to greater values of the heat release, will lie above the complete reaction Hugoniot curve. In this case the Rayleigh line corresponding to the CJ speed does not cross all the relevant Hugoniot curves and the CJ point, C, is a sonic point of incomplete reaction, and no steady solution exists for this speed. The minimum detonation speed, corresponding to the unsupported or self-sustaining detonation wave speed, is then given by the lowest speed for which the corresponding Rayleigh line touches all the relevant Hugoniot curves. This is given by the Rayleigh line corresponding to $D = D^p$ in figure 1, which is just tangent to the Hugoniot curve corresponding to the maximum heat release in the reaction zone, $Q = Q_{max}$, at the pathological point, P. Since the Rayleigh line is tangent to a Hugoniot curve at P the flow is sonic there. We call the detonation corresponding to this speed the pathological detonation. Note that the pathological detonation speed depends on the form of the reaction rates, whereas the CJ speed does not.

Along the Rayleigh line for the pathological speed the steady solution moves down the line from the Neumann point N to the pathological point P, where simultaneously the flow is sonic and the heat release has a maximum value. The solution can then proceed down the supersonic (weak) part of the Rayleigh line if the detonation is unsupported, to the weak equilibrium point W. Alternatively it may proceed back up the subsonic (strong) part of the Rayleigh line for a supported pathological detonation to the strong equilibrium point S.

For supported detonations with speeds greater than the pathological speed, which we shall call overdriven, the steady solution proceeds down the corresponding Rayleigh line, e.g. the line corresponding to $D = D^o$ in figure 1, from the Neumann point N, until it meets the Hugoniot curve of the maximum heat release at M, which, in general, depends on the detonation speed. It then proceeds back up the Rayleigh line to the strong equilibrium point S on the complete reaction Hugoniot curve. Note that in this case there is no path to the weak equilibrium point W. The steady solution is then entirely subsonic throughout and the thermodynamic quantities have a turning point inside the wave.

3.2. *Governing equations of the steady solution*

In terms of our non-dimensional variables, the steady detonation is assumed to travel at unit speed in the positive x-direction in the laboratory frame. We transform to a frame moving with the shock, i.e.

$$x = x^l - t, \quad u = u^l - 1,$$

where x^l and u^l are the position and x-component of the fluid velocity in the laboratory frame. The shock is now stationary at $x = 0$ and the detonation wave lies in the negative x half-plane.

Conservation of mass and momentum then give

$$\rho_0 u_0 = -1, \quad p_0 + \rho_0 u_0^2 = p_- + 1,$$

which allows us to write the thermodynamic variables in terms of u_0 alone:

$$\rho_0 = -\frac{1}{u_0}, \quad p_0 = p_- + 1 + u_0.$$

The sonic value of u_0 can then be found from

$$\eta_0 = c_0^2 - u_0^2 = -\gamma(p_- + 1 + u_0)u_0 - u_0^2 = 0,$$

which gives

$$u_0^s = -\frac{\gamma(p_- + 1)}{\gamma + 1}.$$

Conservation of energy gives

$$\frac{\gamma p_0}{(\gamma - 1)\rho_0} + \tfrac{1}{2}u_0^2 = \tfrac{1}{2} + \frac{\gamma p_-}{(\gamma - 1)} + Q_0,$$

where

$$Q_0 = q_1(1 - \lambda_{10}) + q_2(1 - \lambda_{20}).$$

This gives a relation between the thermodynamic and chemical variables:

$$Q_0 = -\frac{(u_0 + 1)}{2(\gamma - 1)}\left[(\gamma + 1)u_0 + 2\gamma p_- + \gamma - 1\right] \tag{3.1a}$$

or

$$u_0 = -\frac{\gamma(p_- + 1)}{\gamma + 1} \pm \frac{\left[(1 - \gamma p_-)^2 - 2(\gamma^2 - 1)Q_0\right]^{1/2}}{\gamma + 1}$$

$$= u_0^s \pm \frac{\left[2(\gamma^2 - 1)(Q_0^s - Q_0)\right]^{1/2}}{\gamma + 1}, \tag{3.1b}$$

so that u_0 and hence the other thermodynamic variables are double valued for a given value of the total heat release, everywhere except at a sonic point. The thermodynamic quantities therefore have a subsonic, or strong, branch corresponding to the plus sign and a supersonic, or weak, branch corresponding to the minus sign and the solution can only pass from one branch to the other at a sonic point. Note that

$$\frac{\mathrm{d}Q_0}{\mathrm{d}u_0} = \frac{\eta_0}{(\gamma - 1)u_0}$$

so that

$$\frac{\mathrm{d}u_0}{\mathrm{d}x} = \frac{u_0(\gamma - 1)}{\eta_0}\frac{\mathrm{d}Q_0}{\mathrm{d}x},$$

which diverges at a sonic point unless $\mathrm{d}Q_0/\mathrm{d}x = 0$ there, i.e the total heat release must be a maximum there, otherwise no steady solution can exist.

At the shock $\lambda_{10} = \lambda_{20} = 1$, $Q_0 = 0$ and the flow is subsonic so that

$$u_{0+} = \frac{1 - 2\gamma p_- - \gamma}{\gamma + 1}.$$

The weak branch gives $u_0 = -1$ at $x = 0$, i.e. it corresponds to an unshocked state.

At the end of the reaction zone $\lambda_{10} = \lambda_{20} = 0$ and $Q_0 = q_1 + q_2$ which gives

$$u_0^\infty = -\frac{\gamma(p_- + 1)}{\gamma + 1} \pm \frac{\left[(1 - \gamma p_-)^2 - 2(\gamma^2 - 1)(q_1 + q_2)\right]^{1/2}}{\gamma + 1}.$$

The CJ condition is that the flow is sonic for the complete reaction value of Q_0, which gives

$$q_1^{CJ} + q_2^{CJ} = \frac{(1 - \gamma p_-^{CJ})^2}{2(\gamma^2 - 1)}.$$

We define the degree of overdrive, f, by

$$f = \left(\frac{\bar{D}}{\bar{D}^{CJ}}\right)^2,$$

i.e. with respect to the CJ speed. Then

$$p_- = \frac{p_-^{CJ}}{f}, \quad q_i = \frac{q_i^{CJ}}{f}, \quad \tau_i = \frac{\tau_i^{CJ}}{f} \quad (i = 1, 2).$$

For the one-dimensional steady solution, the rate equations become

$$\left.\begin{aligned} \frac{\mathrm{d}\lambda_{10}}{\mathrm{d}x} &= -\frac{\alpha_1\lambda_{10}}{u_0}\exp\left(\tau_1/((p_- + u_0 + 1)u_0)\right), \\ \frac{\mathrm{d}\lambda_{20}}{\mathrm{d}x} &= \frac{\alpha_2(\lambda_{10} - \lambda_{20})}{u_0}\exp\left(\tau_2/((p_- + u_0 + 1)u_0)\right), \end{aligned}\right\} \tag{3.2}$$

with u_0 given by equation (3.1b). Alternatively, we can also use λ_{10} as the independent variable, in which case we have

$$\frac{\mathrm{d}\lambda_{20}}{\mathrm{d}\lambda_{10}} = \frac{\alpha(\lambda_{20} - \lambda_{10})}{\lambda_{10}}\exp\left((\tau_2 - \tau_1)/((p_- + u_0 + 1)u_0)\right). \tag{3.3}$$

Note that in $\lambda_{10}, \lambda_{20}$ space the structure of the solution, and the pathological speed, depend only on the ratio of rate constants, α, and the difference in activation temperatures, $\tau_1 - \tau_2$.

The scale factor α_1 is given by

$$\alpha_1 = \int_0^{1/2} \frac{u_0}{\lambda_{10}}\exp\left(-\tau_1/((p_- + u_0 + 1)u_0)\right)\mathrm{d}\lambda_{10}. \tag{3.4}$$

Integrating equation (3.4) together with equation (3.3) gives α_1. We use a fourth-order Runge–Kutta routine with adaptive step doubling to perform all the integrations in this paper.

Using equation (3.1a) to write λ_{20} in terms of λ_{10} and u_0, we obtain

$$\frac{\mathrm{d}u_0}{\mathrm{d}\lambda_{10}} = \frac{(\gamma - 1)u_0}{\eta_0\lambda_{10}}\left(\alpha[Q_0 - (q_1 + q_2)(1 - \lambda_{10})]\exp\left(\frac{\tau_2 - \tau_1}{(p_- + u_0 + 1)u_0}\right) - q_1\lambda_{10}\right), \tag{3.5}$$

with Q_0 given by equation (3.1a).

The pathological condition is that the flow is sonic when the thermicity is zero, i.e. when $\mathrm{d}Q_0/\mathrm{d}x = 0$. Since

$$\frac{\mathrm{d}Q_0}{\mathrm{d}x} = -q_1\frac{\mathrm{d}\lambda_{10}}{\mathrm{d}x} - q_2\frac{\mathrm{d}\lambda_{20}}{\mathrm{d}x}$$

this gives the values of λ_{10} and λ_{20} at the pathological point:

$$\lambda_{10}^p = \frac{\beta[Q_0^s - (q_1 + q_2)]}{q_1 - \beta(q_1 + q_2)}, \quad \lambda_{20}^p = \frac{(\beta q_2 - q_1)\lambda_{10}^p}{\beta q_2}, \tag{3.6}$$

where

$$\beta_i = \alpha_i\exp\left(\tau_i/((p_- + u_0^s + 1)u_0^s)\right), \quad \beta = \frac{\beta_2}{\beta_1}. \tag{3.7}$$

We use an iterative procedure to find the pathological detonation speed. For a given value of the degree of overdrive, f, we integrate equation (3.5) from the shock into the reaction zone. If f is too small then the solution terminates at a sonic point and

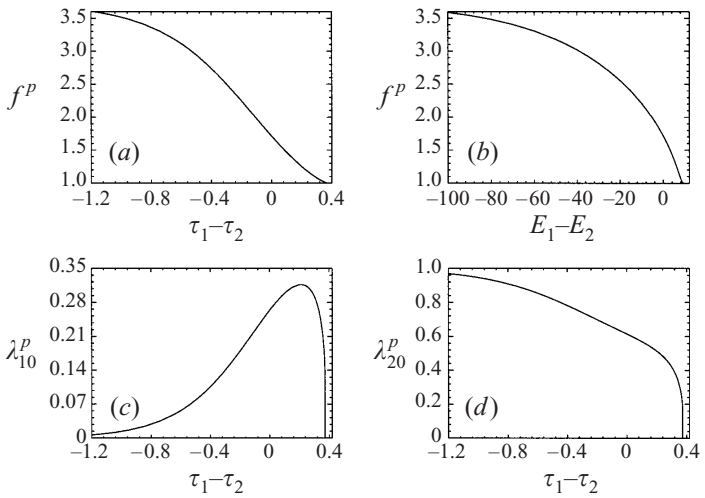

FIGURE 2. (*a*) Pathological degree of overdrive, f^p, versus the difference in activation temperatures, $\tau_1-\tau_2$, (*b*) f^p versus E_1-E_2, (*c*) and (*d*) values of the reaction progress variables at the pathological point versus the difference in activation temperatures. $Q_1=100$, $Q_2=-75$, $\alpha=1$, $\gamma=1.2$.

there is no steady solution, whereas if f is too large the solution corresponds to an overdriven detonation, which reaches a maximum value of the heat release and then proceeds to the strong equilibrium point. We thus obtain upper and lower bounds for the pathological degree of overdrive, f^p, and we can use these to iterate using bisection to obtain f^p to any desired degree of accuracy. A check on the convergence is given by the value of λ_{10} and λ_{20} as predicted by equation (3.6) for the current value of f compared to the values at the sonic point or at the maximum of the heat release.

Figure 2(*a*) shows the variation of the pathological degree of overdrive with the difference in the activation temperatures using our scalings, figure 2(*b*) shows the same thing for Erpenbeck's scaling, while figures 2(*c*) and 2(*d*) show the values of λ_{10} and λ_{20}, respectively, at the pathological point against $\tau_1-\tau_2$. For $\tau_1 \ll \tau_2$ the induction time of the second reaction is much longer than that of the first reaction, so that the endothermic stage begins when the exothermic first reaction is virtually complete, i.e. $\lambda_{10}^p \to 0$, $\lambda_{20}^p \to 1$ as $\tau_1-\tau_2 \to -\infty$. On the other hand, for $\tau_1 \gg \tau_2$ the second reaction has a faster rate than the first so that the burning can remain exothermic throughout and the self-sustaining detonation is then CJ, with no pathological point. This occurs for $\tau_1-\tau_2 > 0.3725$, which corresponds to $E_1-E_2 > 9.067$.

3.3. *Asymptotic solution near the pathological point*

Once the pathological detonation speed has been found, it remains to determine the complete steady structure beyond the sonic point. It is also good practice to integrate away from sonic points. In order to do so we find asymptotic expansions for the steady variables near the pathological point on each branch of the solution and integrate either to the shock or to an equilibrium point. These asymptotic solutions will also be needed in the linear stability analysis.

Consider the branch of the solution between the shock and the pathological point. We define a new variable

$$w = \lambda_{10} - \lambda_{10}^p$$

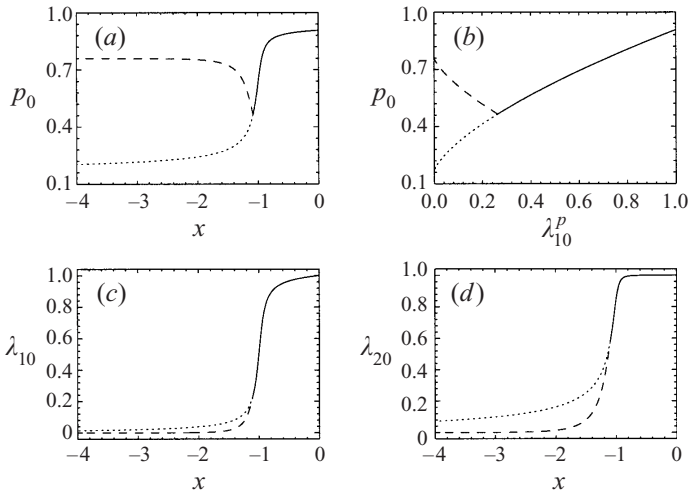

FIGURE 3. Steady pathological detonation with $E_1 = 50$, $E_2 = 50$, $Q_1 = 100$, $Q_2 = -75$, $\alpha = 1$, $\gamma = 1.2$, $f = f^p = 1.7157555$. (*a*) Pressure, p_0, versus distance behind shock, x, (*b*) p_0 versus λ_{10}, (*c*) and (*d*) reaction progress variables versus distance behind shock. The solid line is the branch of the solution between the shock and the pathological point, the dashed line is the branch between the pathological point and the strong equilibrium point and the dotted line is the branch between the pathological point and weak equilibrium point.

so that w is small near the pathological point, and expand λ_{20} in terms of w as

$$\lambda_{20} = \lambda_{20}^p + l_1 w + l_2 w^2 + l_3 w^3 + \ldots,$$

where

$$l_i = \frac{1}{i!}\left(\frac{\mathrm{d}^i \lambda_{20}}{\mathrm{d}w^i}\right)^p = \frac{1}{i!}\left(\frac{\mathrm{d}^i \lambda_{20}}{\mathrm{d}\lambda_{10}^i}\right)^p$$

with $l_1 = -q_1/q_2$ since $\mathrm{d}Q_0/\mathrm{d}w = 0$ at the pathological point. Expanding equation (3.1*b*) then gives

$$u_0 = u_0^s + \left(\frac{2(\gamma-1)q_2 l_2}{\gamma+1}\right)^{1/2} w + \ldots$$

so that

$$l_2 = \frac{(\gamma+1)}{2(\gamma-1)q_2}\left[\left(\frac{\mathrm{d}u_0}{\mathrm{d}w}\right)^p\right]^2.$$

Substituting into equation (3.3) and comparing powers of w gives the l_i. At $O(w)$ we obtain

$$\frac{(\gamma+1)}{(\gamma-1)q_2}\left[\left(\frac{\mathrm{d}u_0}{\mathrm{d}w}\right)^p\right]^2 + \frac{\gamma(\gamma-1)q_1(\tau_1-\tau_2)}{q_2(u_0^s)^3}\left(\frac{\mathrm{d}u_0}{\mathrm{d}w}\right)^p + \frac{\beta(q_1+q_2)-q_1}{q_2\lambda_{10}^p} = 0. \quad (3.8)$$

Since $(\mathrm{d}u_0/\mathrm{d}w)^p > 0$ on the branch between the shock and the pathological point, we must take the positive root.

Similarly, we can obtain asymptotic solutions in terms of w near the pathological point on the branches of the solution between the pathological point and the strong and weak equilibrium points.

We can then use these asymptotic solutions as initial conditions with which to integrate equations (3.2) away from the sonic pathological point. Figure 3 shows the

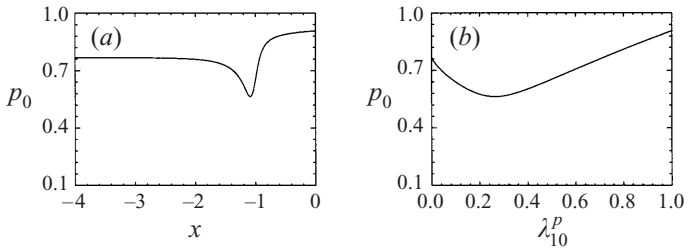

FIGURE 4. Steady overdriven detonation with $E_1 = 50$, $E_2 = 50$, $Q_1 = 100$, $Q_2 = -75$, $\alpha = 1$, $\gamma = 1.2$, $f = 1.8$. (*a*) Pressure, p_0, versus distance behind shock, x, (*b*) p_0 versus λ_{10}.

steady solution for both the supported and unsupported pathological detonations when $E_1 = E_2 = 50$ ($f^p = 1.7157555$). Note that for the supported pathological detonation, which goes to the strong equilibrium point, there is a discontinuity in the derivatives of the thermodynamic quantities at the pathological point. Note also that the unsupported pathological detonation takes much longer to reach equilibrium compared to the supported detonation due to lower temperatures. Figure 4 shows the steady solution for an overdriven detonation with $E_1 = E_2 = 50$, $f = 1.8$. For overdriven detonations the thermodynamic variables have a minimum inside the reaction zone, but their derivatives are continuous there. The structure of the supported pathological detonation is the limit of the structure of overdriven detonations as $f \to f^p$ from above.

4. The linearized equations

Suppose that the one-dimensional steady solution is perturbed so that the position of the (perturbed) shock in the laboratory frame has the form

$$X(y,t) = t + \epsilon e^{\sigma t} e^{iky}, \quad \epsilon \ll 1,$$

i.e. a perturbation in the y-direction.

We transform to a frame moving with the perturbed shock:

$$x = x^l - X(y,t), \quad y = y^l, \quad t = t^l, \quad u = u^l - V(y,t),$$

where

$$V(y,t) = \frac{\partial X}{\partial t}$$

is the velocity of the perturbed shock in the x-direction.

We assume that the perturbed variables are of the form

$$q(x,y,t) = q_0(x) + \epsilon q_1(x) e^{\sigma t} e^{iky},$$

where q is one of ρ, u, v, p, λ_1 or λ_2, and we expand $W_1 \equiv W_1(p,\rho,\lambda_1)$ and $W_2 \equiv W_2(p,\rho,\lambda_1,\lambda_2)$ as

$$W_i = W_{i0}(x) + \epsilon W_{i0,\rho}\rho_1(x)e^{\sigma t}e^{iky} + \epsilon W_{i0,p}p_1(x)e^{\sigma t}e^{iky} + \epsilon W_{i0,\lambda_1}\lambda_1(x)e^{\sigma t}e^{iky} + \epsilon W_{i0,\lambda_2}\lambda_2(x)e^{\sigma t}e^{iky} + \ldots$$

where $W_{i0,\rho} = \partial W_{i0}/\partial\rho_0$, etc.

Note that in the laboratory frame $\partial/\partial x^l$, $\partial/\partial y^l$ and $\partial/\partial t^l$ become

$$\frac{\partial}{\partial x}, \quad \frac{\partial}{\partial y} - \frac{\partial X}{\partial y}\frac{\partial}{\partial x} \quad \text{and} \quad \frac{\partial}{\partial t} - \frac{\partial X}{\partial t}\frac{\partial}{\partial x}$$

in the transformed coordinates and u^l is replaced by

$$u + \frac{\partial X}{\partial t}.$$

Using these and substituting the expressions for the perturbed quantities into equations (2.1), after linearizing in ϵ, the equations can be written in the form

$$\eta_0 \frac{\mathrm{d}\boldsymbol{u}}{\mathrm{d}x} = \boldsymbol{A}\boldsymbol{u} + \boldsymbol{s}, \tag{4.1}$$

where

$$\boldsymbol{u} = (\rho_1, u_1, v_1, p_1, \lambda_{11}, \lambda_{21})^T,$$

$$\boldsymbol{A} = \begin{pmatrix} (-\sigma\eta_0 - a_0^2 u_0' + (\gamma-1)(q_1 W_{10,\rho} + q_2 W_{20,\rho}))/u_0 & (\sigma u_0^2 + (3u_0^2 - a_0^2)u_0')/u_0^3 \\ (-u_0^2 u_0' + (\gamma-1)(q_1 W_{10,\rho} + q_2 W_{20,\rho}))u_0 & (\sigma + 2u_0')u_0 \\ 0 & 0 \\ (-a_0^2 u_0' + (\gamma-1)(q_1 W_{10,\rho} + q_2 W_{20,\rho}))u_0 & (\sigma a_0^2 + (u_0^2 + a_0^2)u_0')/u_0 \\ (u_0\lambda_{10}' - W_{10,\rho})\eta_0 & -\eta_0\lambda_{10}'/u_0 \\ (u_0\lambda_{20}' - W_{20,\rho})\eta_0 & -\eta_0\lambda_{20}'/u_0 \end{pmatrix}$$

$$\begin{pmatrix} -\mathrm{i}k & (\sigma + \gamma u_0' + (\gamma-1)(q_1 W_{10,p} + q_2 W_{20,p}))/u_0 \\ -\mathrm{i}k a_0^2 & (\sigma + \gamma u_0' + (\gamma-1)(q_1 W_{10,p} + q_2 W_{20,p}))u_0 \\ -\sigma\eta_0/u_0 & ik\eta_0 \\ -\mathrm{i}k a_0^2 & (\sigma + \gamma u_0' + (\gamma-1)(q_1 W_{10,p} + q_2 W_{20,p}))u_0 \\ 0 & -\eta_0 W_{10,p} \\ 0 & -\eta_0 W_{20,p} \end{pmatrix}$$

$$\begin{pmatrix} (\gamma-1)(q_1 W_{10,\lambda_1} + q_2 W_{20,\lambda_2})/u_0 & (\gamma-1)q_2 W_{20,\lambda_2}/u_0 \\ (\gamma-1)(q_1 W_{10,\lambda_1} + q_2 W_{20,\lambda_2})u_0 & (\gamma-1)q_2 W_{20,\lambda_2} u_0 \\ 0 & 0 \\ (\gamma-1)(q_1 W_{10,\lambda_1} + q_2 W_{20,\lambda_2})u_0 & (\gamma-1)q_2 W_{20,\lambda_2} u_0 \\ -(\sigma + u_0 W_{10,\lambda_1})\eta_0/u_0 & 0 \\ -\eta_0 W_{20,\lambda_1} & -(\sigma + u_0 W_{20,\lambda_2})\eta_0/u_0 \end{pmatrix}$$

and

$$\boldsymbol{s} = (\sigma^2/u_0, \sigma^2 u_0, -\mathrm{i}k\eta_0 u_0', \sigma^2 a_0^2/u_0, 0, 0)^T,$$

where the prime denotes differentiation with respect to x. Since the steady reaction zone is infinite in length, it is useful to use λ_{10} as the independent variable. Equation (4.1) then becomes

$$-\frac{\alpha_1\lambda_{10}\eta_0}{u_0} \exp\left(\tau_1/((p_- + u_0 + 1)u_0)\right) \frac{\mathrm{d}\boldsymbol{u}}{\mathrm{d}\lambda_{10}} = \boldsymbol{A}\boldsymbol{u} + \boldsymbol{s}. \tag{4.2}$$

Note that equation (4.2) has a singularity whenever $\eta_0 = 0$, i.e. at the pathological point, or $\lambda_{10} = 0$, i.e. at the end of the reaction zone.

4.1. *Boundary conditions*

In the laboratory frame the shock is described by the curve

$$S(x^l, y, t) = x^l - X(y, t) = 0.$$

The unit normal is

$$\boldsymbol{n} = \frac{\nabla S}{|\nabla S|} \quad \text{where} \quad \nabla S = \left(1, -\frac{\partial X}{\partial y}\right),$$

and the normal shock velocity is

$$\boldsymbol{D} = -\frac{\partial S}{\partial t}\frac{\nabla S}{|\nabla S|^2}.$$

Substituting this into the shock conditions (2.2) and linearizing we obtain the boundary conditions at the shock:

$$\left.\begin{aligned} \rho_1(0) = \frac{4\sigma\gamma p_-(\gamma+1)}{(2\gamma p_- + \gamma - 1)^2}, \quad u_1(0) = \frac{\sigma(2\gamma p_- - \gamma + 1)}{(\gamma+1)}, \quad v_1(0) = \frac{2\mathrm{i}k(\gamma p_- - 1)}{(\gamma+1)}, \\ p_1(0) = \frac{4\sigma}{(\gamma+1)}, \quad \lambda_{11}(0) = 0 \quad \lambda_{21}(0) = 0. \end{aligned}\right\} \tag{4.3}$$

The boundary condition to be applied at singular points is that the perturbations are spatially bounded there.

5. Determining the eigenvalues

5.1. *Pathological detonations*

For pathological detonations we seek solutions to equation (4.2) which are asymptotically valid as we approach the sonic point on the branch of the solution between the shock and pathological point. Since $\eta_0 = 0$ at the pathological point equation (4.2) is singular there. We use the methods described by Wasow (1965) for regular singular points to determine these solutions.

Transforming to the independent variable $w = \lambda_{10} - \lambda_{10}^p$, dividing equation (4.2) through by $(\eta_0/w)\mathrm{d}\lambda_{10}/\mathrm{d}x$ since η_0 is $O(w)$ near the pathological point, and expanding the matrix entries in terms of the small quantity w, equation (4.2) can be rewritten in the form

$$w\frac{\mathrm{d}\boldsymbol{u}}{\mathrm{d}w} = \left(\boldsymbol{A}_0 + \boldsymbol{A}_1 w + \boldsymbol{A}_2 w^2 + \ldots\right)\boldsymbol{u} + \boldsymbol{s}_0 + \boldsymbol{s}_1 w + \boldsymbol{s}_2 w^2 + \ldots, \tag{5.1}$$

where now the $\boldsymbol{A}_i$ and $\boldsymbol{s}_i$ are independent of the steady variables, with

$$\boldsymbol{A}_0 = \begin{pmatrix} a_1/(u_0^s)^2 & a_2/(u_0^s)^2 & a_3/(u_0^s)^2 & a_4/(u_0^s)^2 & a_5/(u_0^s)^2 & a_6/(u_0^s)^2 \\ a_1 & a_2 & a_3 & a_4 & a_5 & a_6 \\ 0 & 0 & 0 & 0 & 0 & 0 \\ a_1 & a_2 & a_3 & a_4 & a_5 & a_6 \\ 0 & 0 & 0 & 0 & 0 & 0 \\ 0 & 0 & 0 & 0 & 0 & 0 \end{pmatrix},$$

where

$$a_1 = \frac{(u_0^s)^3(\mathrm{d}u_0/\mathrm{d}w)^p + \gamma(\gamma-1)q_1(\tau_1-\tau_2)}{(\gamma-1)u_0^s(\mathrm{d}u_0/\mathrm{d}w)^p}, \quad a_2 = \frac{\sigma u_0^s - 2\beta_1\lambda_{10}^p(\mathrm{d}u_0/\mathrm{d}w)^p}{(\gamma+1)\beta_1\lambda_{10}^p(\mathrm{d}u_0/\mathrm{d}w)^p},$$

$$a_3 = -\frac{\mathrm{i}k(u_0^s)^2}{(\gamma+1)\beta_1\lambda_{10}^p(\mathrm{d}u_0/\mathrm{d}w)^p},$$

$$a_4 = \frac{\sigma(u_0^s)^4 - \gamma\beta_1\lambda_{10}^p\left[(u_0^s)^3(\mathrm{d}u_0/\mathrm{d}w)^p + \gamma(\gamma-1)q_1(\tau_1-\tau_2)\right]}{(\gamma+1)\beta_1\lambda_{10}^p(u_0^s)^3(\mathrm{d}u_0/\mathrm{d}w)^p},$$

$$a_5 = \frac{(\gamma-1)(q_1-\beta q_2)}{(\gamma+1)\lambda_{10}^p(\mathrm{d}u_0/\mathrm{d}w)^p}, \quad a_6 = \frac{(\gamma-1)\beta q_2}{(\gamma+1)\lambda_{10}^p(\mathrm{d}u_0/\mathrm{d}w)^p}$$

(β_1, β are given by equation (3.7) and $(\mathrm{d}u_0/\mathrm{d}w)^p$ is defined by equation (3.8)), and

$$s_0 = \left(\frac{\sigma^2}{(\gamma+1)\beta_1\lambda_{10}^p u_0^s(\mathrm{d}u_0/\mathrm{d}w)^p}, \frac{\sigma^2 u_0^s}{(\gamma+1)\beta_1\lambda_{10}^p(\mathrm{d}u_0/\mathrm{d}w)^p}, 0, \frac{\sigma^2 u_0^s}{(\gamma+1)\beta_1\lambda_{10}^p(\mathrm{d}u_0/\mathrm{d}w)^p}, 0, 0\right)^T.$$

5.1.1. *Solution of the homogeneous equation*

The eigenvalues of the matrix $\boldsymbol{A}_0$ are h, 0, 0, 0, 0, 0, where

$$h = \frac{2\sigma(u_0^s)^4 - \beta_1\lambda_{10}^p\left[(\gamma+1)(u_0^s)^3(\mathrm{d}u_0/\mathrm{d}w)^p + \gamma(\gamma-1)^2 q_1(\tau_1-\tau_2)\right]}{(\gamma+1)\beta_1\lambda_{10}^p(u_0^s)^3(\mathrm{d}u_0/\mathrm{d}w)^p}.$$

Since none of the eigenvalues of $\boldsymbol{A}_0$ differ by a positive integer we can find a transformation of the form

$$\boldsymbol{u} = \left(\boldsymbol{T}_0 + \boldsymbol{T}_1 w + \boldsymbol{T}_2 w^2 + \ldots\right)\boldsymbol{z},$$

where $\boldsymbol{T}_0$ is the matrix whose columns are the eigenvectors of $\boldsymbol{A}_0$, which reduces the homogeneous form of equation (5.1) to

$$w\frac{\mathrm{d}\boldsymbol{z}}{\mathrm{d}w} = \boldsymbol{B}_0\boldsymbol{z}, \tag{5.2}$$

where

$$\boldsymbol{B}_0 = \begin{pmatrix} h & 0 & 0 & 0 & 0 & 0 \\ 0 & 0 & 0 & 0 & 0 & 0 \\ 0 & 0 & 0 & 0 & 0 & 0 \\ 0 & 0 & 0 & 0 & 0 & 0 \\ 0 & 0 & 0 & 0 & 0 & 0 \\ 0 & 0 & 0 & 0 & 0 & 0 \end{pmatrix}.$$

Equation (5.2) has the six independent solutions

$$\boldsymbol{z}_1 = (0,1,0,0,0,0)^T, \quad \boldsymbol{z}_2 = (0,0,1,0,0,0)^T, \quad \boldsymbol{z}_3 = (0,0,0,1,0,0)^T,$$

$$\boldsymbol{z}_4 = (0,0,0,0,1,0)^T, \quad \boldsymbol{z}_5 = (0,0,0,0,0,1)^T, \quad \boldsymbol{z}_6 = (w^h,0,0,0,0,0)^T.$$

Transforming back to the variables $\boldsymbol{u}$ we have six independent, homogeneous, asymptotic solutions of the form

$$\boldsymbol{u}_i = \boldsymbol{a}_0^i + \boldsymbol{a}_0^i w + \boldsymbol{a}_0^i w^2 + \ldots, \quad i = 1,\ldots,5,$$

$$\boldsymbol{u}_6 = w^h\left(\boldsymbol{a}_0^6 + \boldsymbol{a}_0^6 w + \boldsymbol{a}_0^6 w^2 + \ldots\right),$$

where the $\boldsymbol{a}_i^j$ are constant vectors, i.e. they depend only on the parameters.

Now, provided

$$\mathrm{Re}(\sigma) \geqslant \frac{\beta_1\lambda_{10}^p}{2(u_0^s)^4}\left[(\gamma+1)(u_0^s)^3(\mathrm{d}u_0/\mathrm{d}w)^p + \gamma(\gamma-1)^2 q_1(\tau_1-\tau_2)\right] \tag{5.3}$$

(note that the term on the right-hand side of equation (5.3) is negative), then h is negative and thus the solution $\boldsymbol{u}_6$ is unbounded at the pathological point so that the boundedness condition requires that we discard this solution.

The fact that equation (5.3) allows stable modes distinguishes the pathological detonation from CJ and overdriven detonations which formally have no stable modes

when the reaction zone is infinite in length (Sharpe 1997*a*). Bourlioux *et al.* (1991) claim that even when the detonation is infinite in length there are stable modes, and that they are 'resonant acoustic scattering states', with eigenfunctions that grow unboundedly as $x \to -\infty$. For these cases, using a method similar to that described above, one can determine asymptotic solutions valid as $x \to -\infty$ (note that Bourlioux *et al.* 1991 give incorrect forms of these asymptotic solutions, the correct ones are given in Sharpe 1997*a*). For $\mathrm{Re}(\sigma) \geqslant 0$ there is one unbounded solution, which must be discarded, while for $\mathrm{Re}(\sigma) < 0$ this solution becomes bounded, but the remaining solutions all become unbounded. Hence for $\mathrm{Re}(\sigma) < 0$ there is only one valid solution and the eigenvalue problem is overdetermined, so that there are no stable modes. However, Bourlioux *et al.* (1991) use Lee & Stewart's (1990) method to instead integrate the linearized equations from the shock into the reaction zone and apply a condition at a large distance from the shock. For $\mathrm{Re}(\sigma) \geqslant 0$ this condition is simply that the solution is independent of the unbounded solution, and so is equivalent to the method used by Sharpe (1997*a*). For $\mathrm{Re}(\sigma) < 0$, Bourlioux *et al.* (1991) continue to use the same downstream boundary condition to find 'stable modes'. They remark that even though all but one of the solutions are now growing as $x \to -\infty$, their condition eliminates the fastest growing mode. In fact it does not, it now ensures that the solution is independent of the only bounded solution, and so is the worst possible condition to use. It is no wonder that the 'eigenfunctions' of these spurious stable modes grow unboundedly! In fact for any non-eigenvalue value of σ (whether $\mathrm{Re}(\sigma)$ is positive or negative) the corresponding 'eigenfunctions' will be spatially growing since they contain parts of unbounded solutions. Such unbounded solutions are totally incompatible with a linear stability analysis since the perturbations are assumed to be small, and unbounded perturbations are not small in any sense. However, this is not too important since in reality there must be some boundary at a *finite* distance behind the shock, where the perturbations will be constrained to be bounded and hence stable modes will exist. Indeed, one-dimensional time-dependent numerical calculations, where the boundary condition at the downstream end of the numerical domain constrains the perturbations to be zero there, do have stable modes for CJ and overdriven detonations which are formally of infinite length.

5.1.2. *Solution of the inhomogeneous equation*

To solve the inhomogeneous equation, (5.1), we transform to the variables

$$\boldsymbol{q} = \boldsymbol{T}_0^{-1}\boldsymbol{u}$$

so that the equation is then of the form

$$w\frac{\mathrm{d}\boldsymbol{q}}{\mathrm{d}w} = \left(\boldsymbol{B}_0 + \boldsymbol{B}_1 w + \boldsymbol{B}_2 w^2 + \ldots\right)\boldsymbol{q} + \boldsymbol{r}_0 + \boldsymbol{r}_0 w + \boldsymbol{r}_0 w^2 + \ldots,$$

where

$$\boldsymbol{r}_i = \boldsymbol{T}_0^{-1}\boldsymbol{s}_i$$

with

$$\boldsymbol{r}_0 = \left(\frac{\sigma^2}{(\gamma+1)\beta_1\lambda_{10}u_0^s(\mathrm{d}u_0/\mathrm{d}w)^p}, 0, 0, 0, 0, 0\right)^T. \tag{5.4}$$

We can find a particular integral of equation (5.4) of the form

$$\boldsymbol{q}_P = \boldsymbol{c}_0 + \boldsymbol{c}_1 w + \boldsymbol{c}_2 w^2 + \ldots,$$

where the $\boldsymbol{c}_i$ are found by substituting into equation (5.4) and comparing the coefficients of powers of w, with

$$\boldsymbol{c}_0 = \left(-\frac{\sigma^2}{(\gamma+1)\beta_1\lambda_{10}u_0^s(\mathrm{d}u_0/\mathrm{d}w)^p h}, 0, 0, 0, 0, 0 \right)^T.$$

Transforming back to $\boldsymbol{u}$ gives a particular integral of the form

$$\boldsymbol{u}_P = \boldsymbol{a}_0^P + \boldsymbol{a}_1^P w + \boldsymbol{a}_2^P w^2 + \ldots,$$

where the $\boldsymbol{a}_i^P$ are constant vectors.

5.1.3. *Determining the linear modes*

We now have an asymptotic solution of the form

$$\boldsymbol{u} \sim b_1\boldsymbol{u}_1 + b_2\boldsymbol{u}_2 + b_3\boldsymbol{u}_3 + b_4\boldsymbol{u}_4 + b_5\boldsymbol{u}_5 + \boldsymbol{u}_P$$

as $w \to 0$, where the b_i are (complex) constants of integration ($b_j = b_j^R + \mathrm{i}b_j^I$, say), and at the shock we have, from the linearized shock conditions (4.3), $\boldsymbol{u} = \boldsymbol{u}_S$, where

$$\boldsymbol{u}_S = \left(\frac{4\sigma\gamma p_-(\gamma+1)}{(2\gamma p_- + \gamma - 1)^2}, \frac{\sigma(2\gamma p_- - \gamma + 1)}{(\gamma+1)}, \frac{2\mathrm{i}k(\gamma p_- - 1)}{(\gamma+1)}, \frac{4\sigma}{(\gamma+1)}, 0, 0 \right)^T.$$

We can therefore integrate the full equation for $\boldsymbol{u}$, equation (4.2), using the asymptotic solutions, $\boldsymbol{u}_i$ of the homogeneous equation or $\boldsymbol{u}_p$ of the inhomogeneous equation, as initial conditions, together with equation (3.5) with the asymptotic expansion for u_0 as the initial condition, until we reach the shock at $\lambda_{10} = 1$.

We have ten constants of integration (the b_i^R and b_i^I) and twelve conditions at the shock (the real and imaginary parts of the components of $\boldsymbol{u}_S$), so only for discrete values of the complex quantity σ, the eigenvalues, will all the conditions be satisfied for given values of the other parameters. Given a trial value of σ, we integrate the solutions to the shock and obtain $\boldsymbol{u}_i(\lambda_{10} = 1) = \boldsymbol{u}_{i,0}$, say, and $\boldsymbol{u}_P(\lambda_{10} = 1) = \boldsymbol{u}_{P,0}$. Consider the quantity

$$m = |(b_1^R + \mathrm{i}b_1^I)\boldsymbol{u}_{1,0} + (b_2^R + \mathrm{i}b_2^I)\boldsymbol{u}_{2,0} + (b_2^R + \mathrm{i}b_3^I)\boldsymbol{u}_{3,0} + (b_4^R + \mathrm{i}b_4^I)\boldsymbol{u}_{4,0} + (b_5^R + \mathrm{i}b_5^I)\boldsymbol{u}_{5,0} + \boldsymbol{u}_{P,0} - \boldsymbol{u}_S|^2 \qquad (5.5)$$

(where $|\boldsymbol{q}|^2 = \boldsymbol{q} \cdot \bar{\boldsymbol{q}}$). Then if σ is an eigenvalue we can choose the b_i^R and b_i^I such that $m = 0$. For any given σ we can minimize m by partially differentiating (5.5) with respect to each of the b_i^R and b_i^I and setting these quantities to zero, which clearly corresponds to the minimum m given each of the other constants. This gives a 10×10 system of linear equations, $\boldsymbol{C}\boldsymbol{v} = \boldsymbol{b}$ say, where $\boldsymbol{v} = (b_1^R, b_1^I, \ldots, b_5^R, b_5^I)^T$ and $\boldsymbol{C}$ and $\boldsymbol{b}$ are a constant matrix and vector respectively. Solving these for $\boldsymbol{v}$ gives the b_i^R and b_i^I such that m is a minimum.

We iteratively search the real and imaginary σ-space and determine $\min(m)$ at each point in order to find the eigenvalues where $\min(m)$ has local minima. In fact we can iteratively change any two of the parameters, so, for example, to find the neutrally stable wavenumbers, with the other parameters fixed, we can set $\mathrm{Re}(\sigma) = 0$ and search the $(\mathrm{Im}(\sigma), k)$-plane.

In order to check that we have started the integration at a small enough value of w for the asymptotic solutions to give an accurate value of $\min(m)$, we evaluate $\min(m)$ by starting at a value of w and at a value of $w/2$. If these two values are not in agreement to a required tolerance then w is halved and the process repeated.

5.2. *Overdriven detonations*

In order to determine the linear eigenvalues for the overdriven detonations we could find asymptotic solutions valid near the strong equilibrium point. However, a phase-plane analysis of the steady solution about the equilibrium point gives

$$\begin{pmatrix} \lambda_{10} \\ \lambda_{20} \end{pmatrix} \sim C_1 \mathrm{e}^{-\kappa_1 x} \begin{pmatrix} 1 \\ \kappa_2/(\kappa_2-\kappa_1) \end{pmatrix} + C_2 \mathrm{e}^{-\kappa_2 x} \begin{pmatrix} 0 \\ 1 \end{pmatrix} \quad (\kappa_1 \neq \kappa_2)$$

as $x \to -\infty$, where C_1 and C_2 are constants and

$$\kappa_i = \frac{\alpha_i}{u_0^\infty} \exp\left(\tau_1/((p_- + u_0^\infty + 1)u_0^\infty)\right), \quad i = 1, 2,$$

so that λ_{20} is $O(\lambda_{10})$ if $\kappa = \kappa_2/\kappa_1 > 1$ or $O(\lambda_{10}^\kappa)$ if $\kappa < 1$, as $\lambda_{10} \to 0$ (note that for $\kappa \leqslant 1$ the derivative $\mathrm{d}\lambda_{20}/\mathrm{d}\lambda_{10}$ is infinite at the equilibrium point). The asymptotic solutions and the ordering of the higher-order terms would then depend on the value of κ, indeed, for $\kappa < 1$, λ_{10} would not be a suitable independent variable for the asymptotic expansions. Since it would be somewhat tedious to determine these different asymptotic solutions and we are only interested in the stability of the overdriven detonations in order to compare the linear spectrum as $f \to f^p$ with the pathological spectrum, we instead use the method of Lee & Stewart (1990).

We integrate equations (3.5) and (4.2) from the shock using the shock conditions (4.3) as initial conditions towards the end of the reaction zone, stopping at a small value of λ_{10} and applying a boundedness or radiation condition there.

We first rewrite equation (4.2) as

$$\lambda_{10} \frac{\mathrm{d}\boldsymbol{u}}{\mathrm{d}\lambda_{10}} = \boldsymbol{A}_* \boldsymbol{u} + \boldsymbol{s}_*.$$

where

$$\boldsymbol{A}_* = -\frac{u_0}{\alpha_1 \eta_0} \exp\left(-\tau_1/((p_- + u_0 + 1)u_0)\right) \boldsymbol{A},$$

$$\boldsymbol{s}_* = -\frac{u_0}{\alpha_1 \eta_0} \exp\left(-\tau_1/((p_- + u_0 + 1)u_0)\right) \boldsymbol{s}.$$

Then we have

$$\boldsymbol{A}_*^\infty = \frac{1}{\kappa_1 \eta_0^\infty} \begin{pmatrix} \sigma\eta_0^\infty/u_0^\infty & -\sigma/u_0^\infty & \mathrm{i}k & -\sigma/u_0^\infty \\ 0 & -\sigma u_0^\infty & \mathrm{i}k(a_0^\infty)^2 & -\sigma u_0^\infty \\ 0 & 0 & \sigma\eta_0^\infty/u_0^\infty & -\mathrm{i}k\eta_0^\infty \\ 0 & -\sigma(a_0^\infty)^2/u_0^\infty & \mathrm{i}k(a_0^\infty)^2 & -\sigma u_0^\infty \\ 0 & 0 & 0 & 0 \\ 0 & 0 & 0 & 0 \end{pmatrix}$$

$$\begin{pmatrix} (\gamma-1)(q_2\kappa_2 - q_1\kappa_1)/u_0^\infty & -(\gamma-1)\kappa_2 q_2/u_0^\infty \\ (\gamma-1)(q_2\kappa_2 - q_1\kappa_1)u_0^\infty & -(\gamma-1)\kappa_2 q_2 u_0^\infty \\ 0 & 0 \\ (\gamma-1)(q_2\kappa_2 - q_1\kappa_1)u_0^\infty & -(\gamma-1)\kappa_2 q_2 u_0^\infty \\ (\sigma/u_0^\infty + \kappa_1)\eta_0^\infty & 0 \\ -\kappa_2\eta_0^\infty & (\sigma/u_0^\infty + \kappa_2)\eta_0^\infty \end{pmatrix},$$

which has eigenvalues h_1, h_1, h_1+1, $h_1+\kappa$, h_2 and h_3, where

$$h_1 = \frac{\sigma}{\kappa_1 u_0^\infty}, \quad h_2 = -\frac{\sigma u_0^\infty + a_0^\infty \left(\sigma^2 + k^2 \eta_0^\infty\right)^{1/2}}{\kappa_1 \eta_0^\infty},$$

$$h_3 = -\frac{\sigma u_0^\infty - a_0^\infty \left(\sigma^2 + k^2 \eta_0^\infty\right)^{1/2}}{\kappa_1 \eta_0^\infty}.$$

Now, for $\mathrm{Re}(\sigma)\geqslant 0$, $h_3 < 0$ so that the solution corresponding to this eigenvalue is unbounded at the equilibrium point. Note that, because of the integer difference of the eigenvalues, in order to find the asymptotic solutions corresponding to the eigenvalues h_1, h_1 we need higher-order terms in the expansion of $\boldsymbol{A}_*$ (cf. Sharpe 1997*a*), and finding the asymptotic solutions becomes even more complicated whenever κ is an integer. Also note that for $\mathrm{Re}(\sigma)<0$ the eigenvalue problem is overdetermined, so that there are no stable modes for any parameter values, in contrast to the pathological detonation.

The boundedness condition requires that the solution is independent of the unbounded solution corresponding to the eigenvalue h_3, which requires that

$$\boldsymbol{l}\cdot\boldsymbol{u} = 0$$

near the equilibrium point, where

$$\boldsymbol{l} = \left(0, \sigma, -\mathrm{i}ku_0^\infty, \frac{u_0^\infty}{a_0^\infty}\left(\sigma^2 + k^2\eta_0^\infty\right)^{1/2}, l_5, l_6\right)$$

is the left eigenvector of $\boldsymbol{A}_*$ corresponding to the eigenvalue h_3 (here l_5 and l_6 are rather complicated functions of the parameters).

To determine the eigenvalues we integrate the equations from the shock and evaluate the quantity

$$m = |\boldsymbol{l}\cdot\boldsymbol{u}|,$$

then only if σ is an eigenvalue does $m = 0$. We can thus iteratively search the positive real and imaginary σ-space and determine m at each point in order to find the eigenvalues where m has local minima. The value of λ_{10} at which the boundedness condition is applied is chosen to be small enough so that a decrease in this value does not change the value of the eigenvalue.

6. One-dimensional perturbations

We first consider the case of one-dimensional perturbations, i.e. $k = 0$, corresponding to the longitudinal instability.

6.1. *Pathological detonations*

6.1.1. *Neutral stability*

Figure 5 shows the neutral stability curves for the three lowest-frequency modes in the (E_1, E_2)-plane. On these curves $\mathrm{Re}(\sigma) = 0$, and below and to the right of the curves the mode is unstable to one-dimensional perturbations, i.e. $\mathrm{Re}(\sigma) > 0$, while above and to the left of them the mode is stable, i.e. $\mathrm{Re}(\sigma) < 0$. The dashed line is the line $E_1 - E_2 = 9.067$ below which the unsupported steady detonation is of the CJ type. The neutral stability curves of the higher-frequency modes lie within the unstable region of the modes with lower frequency, so that the neutral stability curve of the fundamental (lowest frequency) mode is the neutral stability boundary

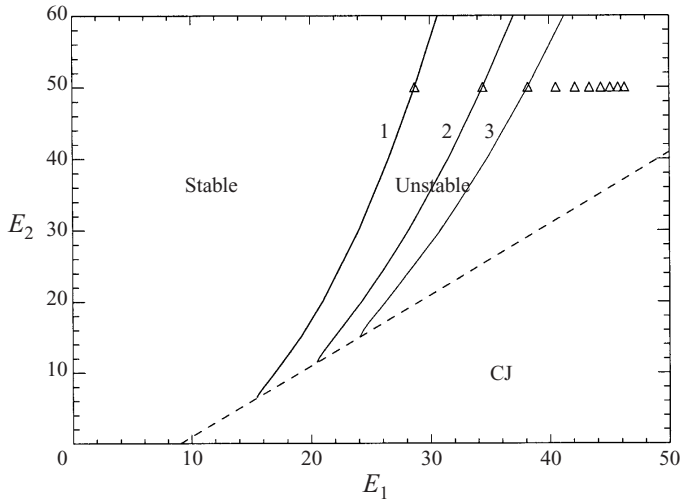

FIGURE 5. Neutral stability curves for the three lowest-frequency modes (numbered in order of ascending frequency) in the (E_1, E_2)-plane for $Q_1 = 100$, $Q_2 = -75$, $\alpha = 1$, $\gamma = 1.2$. Also shown are the first ten neutrally stable modes for $E_2 = 50$ (triangles).

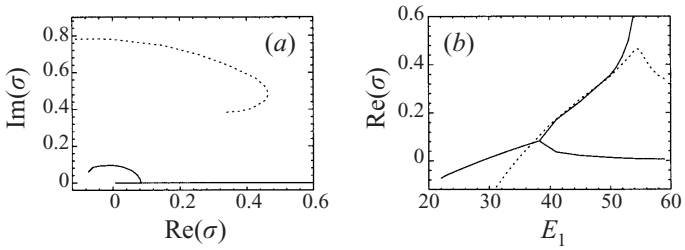

FIGURE 6. Migration of the fundamental mode (solid curve) and the first overtone (dashed curve) as the activation temperature of the first reaction, E_1, is varied for $E_2 = 50$, $Q_1 = 100$, $Q_2 = -75$, $\alpha = 1$, $\gamma = 1.2$. (*a*) Frequencies versus growth rates and (*b*) growth rate versus E_1.

and the detonation itself is unstable (stable) to one-dimensional perturbations if the fundamental mode is unstable (stable). Note that decreasing the value of $E_1 - E_2$ tends to stabilize the detonation.

6.1.2. *Migration of the linear spectrum as the activation temperature of the first reaction is varied*

Figure 6 shows the dependence of the growth rates and frequencies of the fundamental mode and first overtone on E_1 when $E_2 = 50$, up to $E_1 = 59.067$ when the unsupported detonation becomes CJ. The modes are neutrally stable at $E_1 = 28.71$ for the fundamental mode, so that the detonation is stable to one-dimensional perturbations below this value, and at $E_1 = 34.42$ for the first overtone. Note the existence of stable modes for E_1 below these values. The stable eigenvalues become difficult to find as E_1 decreases because the value of $\min(m)$ only converges at very small starting values of w (less than 10^{-6}). As E_1 is increased above 28.71, the growth rate of the fundamental mode increases while its frequency decreases, until it hits the Re(σ)-axis at $E_1 = 38.25$. As E_1 is increased further the mode and its complex conjugate split into two real non-oscillatory eigenvalues, one of which has an increasing growth rate with E_1 and the other a decreasing growth rate. The behaviour of the first overtone is

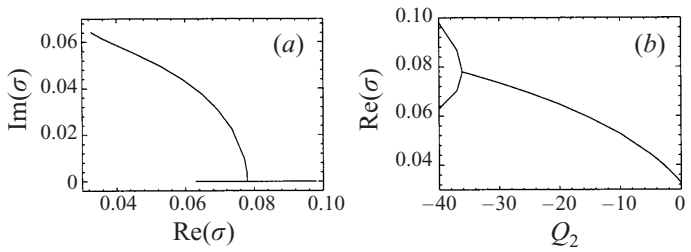

FIGURE 7. Migration of the fundamental mode as the heat of reaction of the second reaction, Q_2, is varied in the range $0 \geqslant Q_2 \geqslant -40$, for $E_1 = 30$, $E_2 = 50$, $Q_1 = 50$, $\alpha = 1$, $\gamma = 1.2$. (*a*) Frequency versus growth rate, (*b*) growth rate versus Q_2.

rather different. As E_1 is increased from its neutrally stable value, the growth rate of this mode increases while its frequency decreases. At $E_1 = 54.55$, however, the growth rate reaches a maximum of 0.464 and then begins to decrease as E_1 increases further.

As the activation temperature is increased, more and more higher-frequency modes become unstable in order of ascending frequency (cf. figure 5). These modes behave in a similar fashion to the first overtone. Note that between about $E_1 = 40$ and $E_1 = 50$ the growth rates of the larger of the non-oscillatory modes and the first overtone are comparable, but above about $E_1 = 50$ the growth rate of the non-oscillatory mode begins to increase very sharply with increasing E_1 so that above this value this is the dominant mode. Apart from the existence of the stable modes, this behaviour is qualitatively the same as for CJ detonations in the idealized case (Sharpe 1997*a*). However note that the pathological degree of overdrive varies with E_1 in figure 6.

6.1.3. *Migration of the linear spectrum as the endothermicity is varied*

We now consider how the stability changes as the endothermicity increases, and specifically how the stability is affected as the self-sustaining detonation changes from being of the CJ type to the pathological type. For $Q_2 = 0$ there is no endothermic stage and the self-sustaining steady wave is CJ. Note that in this case the internal energy does not depend on λ_2, only the rate equation for the second reaction has a λ_2 dependence, and hence the stability is the same as for the idealized one-reaction system. As $|Q_2|$ increases, and the endothermic stage becomes more prominent, the self-sustaining steady detonation becomes pathological, and the sonic point moves into the reaction zone and further towards the shock. Figure 7 shows how the fundamental mode varies as the endothermicity is increased, for $E_1 = 30$, $E_2 = 50$, $Q_1 = 50$ and Q_2 in the range $0 \geqslant Q_2 \geqslant -40$. Figures 8 and 9 show the eigenfunctions for various values of Q_2. Note that for $Q_2 = 0$ (when the self-sustaining detonation is of the CJ type) we determine the linear spectrum using the method described in Sharpe (1997*a*). For no endothermicity there is just one unstable mode, $\sigma = 0.0327 + 0.0642\mathrm{i}$. It can be seen from figure 7 that increasing the endothermicity has the effect of making the detonation more unstable. As $|Q_2|$ increases the growth rate of the fundamental mode increases, while the frequency decreases, until the mode hits the $\mathrm{Re}(\sigma)$-axis at $Q_2 = -36.16$ and then splits into two real eigenvalues. Hence detonations of the CJ type tend to be more stable than those of the pathological type.

6.2. *Overdriven detonations*

6.2.1. *Migration of the linear spectrum as the degree of overdrive is varied*

The structure of the unsupported pathological detonation is different from the structure of the supported detonation as $f \to f^p$, and since we apply the boundedness

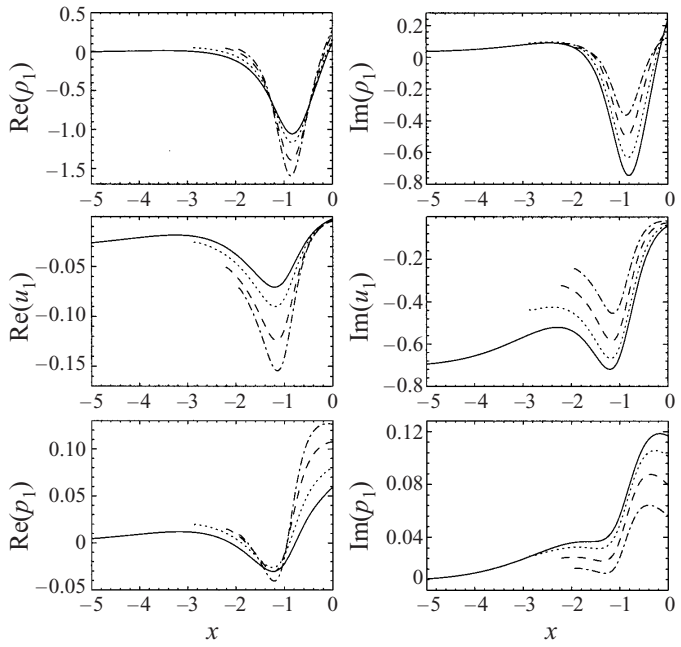

FIGURE 8. Real and imaginary parts of the perturbation eigenfunctions for the density, x-component of velocity and pressure. $E_1 = 30$, $E_2 = 50$, $Q_1 = 50$, $\alpha = 1$, $\gamma = 1.2$, and $Q_2 = 0$ (solid line), $Q_2 = -5$ (dotted line), $Q_2 = -15$ (dashed line) and $Q_2 = -25$ (dot-dashed line).

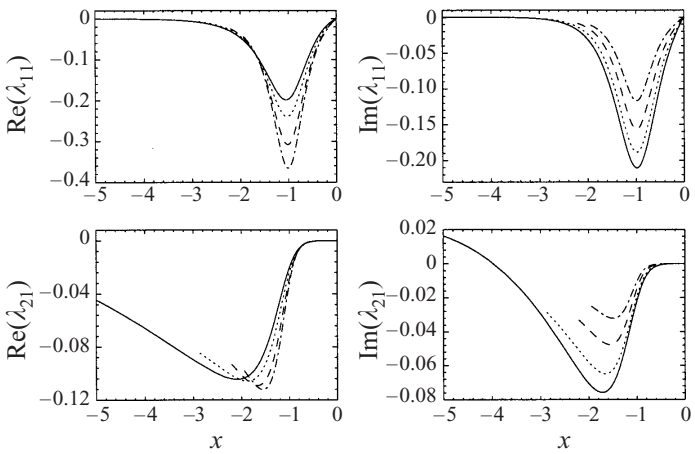

FIGURE 9. Real and imaginary parts of the perturbation eigenfunctions for the reaction progress variables. $E_1 = 30$, $E_2 = 50$, $Q_1 = 50$, $\alpha = 1$, $\gamma = 1.2$, and $Q_2 = 0$ (solid line), $Q_2 = -5$ (dotted line), $Q_2 = -15$ (dashed line) and $Q_2 = -25$ (dot-dashed line).

condition to the linearized equations at different singular points for the pathological and overdriven detonations we now investigate whether the linear spectrum is itself singular. Indeed, the pathological detonation admits stable modes, whereas the overdriven detonations do not. This difference is due to the sonic singular point of pathological detonations being at a finite distance behind the front, whereas the equilibrium singular point is formally at an infinite distance behind the front for

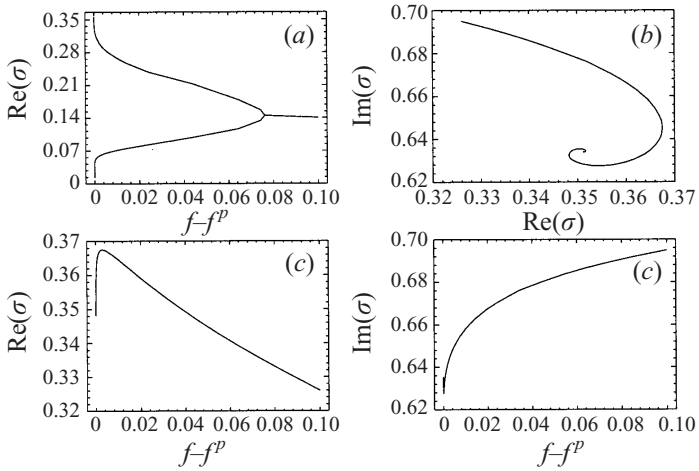

FIGURE 10. Migration of the fundamental mode and first overtone as the degree of overdrive, f, is varied in the range $0 \leqslant f - f^p \leqslant 0.1$, for $E_1 = E_2 = 50$, $Q_1 = 100$, $Q_2 = -75$, $\alpha = 1$, $\gamma = 1.2$. (a) Growth rate versus $f - f^p$ of the fundamental mode, (b) frequency versus growth rate of the first overtone, (c) growth rate versus $f - f^p$ of the first overtone, and (d) frequency versus $f - f^p$ of the first overtone.

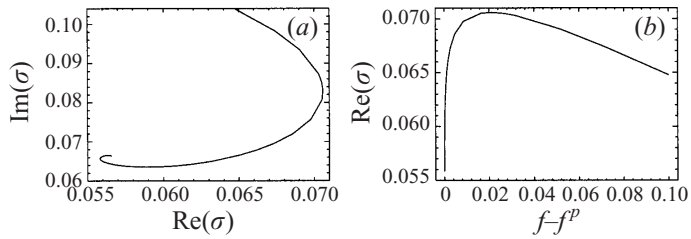

FIGURE 11. Migration of the fundamental mode as the degree of overdrive, f, is varied in the range $0 \leqslant f - f^p \leqslant 0.1$, for $E_1 = 35$, $E_2 = 50$, $Q_1 = 100$, $Q_2 = -75$, $\alpha = 1$, $\gamma = 1.2$. (a) Frequency versus growth rate, (b) growth rate versus $f - f^p$.

overdriven detonations. Hence one may ask whether the unstable modes for the pathological detonation are different from the unstable modes of overdriven detonations as $f \to f^p$. Figure 10, which shows the migration of the two lowest-frequency modes with f near the pathological degree of overdrive for $E_1 = E_2 = 50$, shows that this is not the case. However, the modes are extremely sensitive to f near $f = f^p$ and become increasingly sensitive as $f \to f^p$. The growth rates of the non-oscillatory modes of the pathological detonation increase for the smaller growth rate and decrease for the larger growth rate very sharply as the degree of overdrive increases from its pathological value (these non-oscillatory modes eventually converge into an oscillatory mode). The first overtone meanwhile spirals out from its pathological value very quickly, the spiral evolving with $\log(f - f^p)$. This shows that even a very small change in the degree of overdrive results in a relatively large change in the unstable modes.

Figure 11 shows the migration of the fundamental mode for f in the range $0 \leqslant f - f^p \leqslant 0.1$ for $E_1 = 35$, $E_2 = 50$, when this mode is non-oscillatory for the pathological detonation. Now this mode also spirals out from its pathological value and again the mode is very sensitive to the degree of overdrive near its

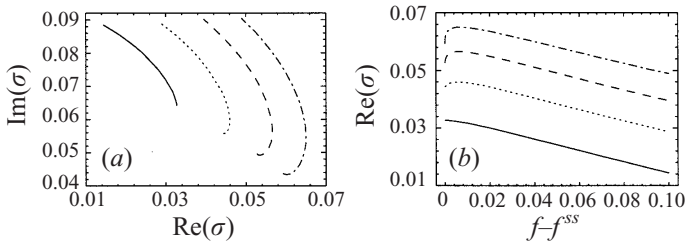

FIGURE 12. Migration of the fundamental mode as the degree of overdrive, f, is varied in the range $0 \leqslant f - f^{ss} \leqslant 0.1$, for $E_1 = 30$, $E_2 = 50$, $Q_1 = 50$, $\alpha = 1$, $\gamma = 1.2$ and $Q_2 = 0$ (solid line), $Q_2 = -5$ (dotted line), $Q_2 = -10$ (dashed line) and $Q_2 = -15$ (dot-dashed line). (*a*) Frequency versus growth rate, (*b*) growth rate versus $f - f^{ss}$.

pathological value. The linear mode has a frequency of 0.06637 for the pathological detonation, which corresponds to a period of oscillation of 94.67, while for an overdriven detonation with $f - f^{p} = 0.01$ the frequency is 0.07659, which corresponds to a period of 82.04, i.e. a 0.4% difference in the degree of overdrive results in a 13% change in the period.

6.2.2. *Change in the dependence on the degree of overdrive as the endothermicity is varied*

The behaviour of the migrating modes with the degree of overdrive described above for pathological detonations is quite different than for CJ type detonations, for which the modes are not at all sensitive near the minimum, i.e. CJ or $f = 1$, degree of overdrive, and the growth rates and frequencies of oscillatory modes depend almost linearly on f for not too unstable modes (Sharpe 1997*b*; Short 1997). Hence for the idealized CJ detonation increasing the degree of overdrive stabilizes the detonation to one-dimensional perturbations, i.e. the growth rates of the mode decrease. However, figures 10 and 11 show that increasing the degree of overdrive can actually make the detonation more unstable than the pathological detonation. Indeed, for cases where a mode is very near the stability boundary for the pathological detonation, on whichever side, as the degree of overdrive is increased there can be alternating ranges of f for which the one-dimensional mode is stable/unstable due to the spiral nature of the migrating mode. Most remarkable is the fact that the unsupported pathological detonation can be stable to one-dimensional perturbation, but there can be a range of corresponding overdriven detonations which are unstable.

How does this change in behaviour with the degree of overdrive unfold as the self-sustaining detonation changes from the CJ type to the pathological type (e.g. as the endothermicity is increased)? Figure 12 shows the dependence on the degree of overdrive of the fundamental mode for $E_1 = 30$, $E_2 = 50$, $Q_1 = 50$ and values of $Q_2 = 0$, -5, -10 and -15. In each case the degree of overdrive was varied in the range $0 \leqslant f - f^{ss} \leqslant 0.1$, where

$$f^{ss} = \begin{cases} f^{CJ} = 1, & Q_2 = 0 \\ f^{p} > 1, & Q_2 < 0 \end{cases}$$

is the self-sustaining degree of overdrive. For $Q_2 = 0$ the self-sustaining detonation is of the CJ type. In this case (solid line in figure 12) the growth rate decreases monotonically with the degree of overdrive, while the frequency increases monotonically. The linear spectrum is not especially sensitive near $f = 1$. For $Q_2 = -5$ (dotted line in figure 12) the self-sustaining detonation is pathological. In this case the growth rate

now increases slightly as f increases away from f^p before reaching a maximum and then decreasing, while the frequency still increases monotonically. For lower vales of Q_2 (e.g. the dashed and dot-dashed lines in figure 12, which correspond to $Q_2 = -10$ and $Q_2 = -15$, respectively), the frequency initially decreases, and the spiral nature of the migrating mode becomes more pronounced. Note that as the degree of endothermicity increases, the sensitivity of the mode near $f = f^p$ also becomes more pronounced.

7. Multi-dimensional perturbations

7.1. *Pathological detonations*

We now consider the case of multi-dimensional perturbations. Note that our choice of two-dimensional perturbations also covers the case of three-dimensional perturbations, since if we have three-dimensional perturbations of the form $\epsilon q_1(x)\mathrm{e}^{\sigma t}\mathrm{e}^{k_1 y}\mathrm{e}^{k_2 z}$, we can simply choose a new transverse direction, y', with wavenumber $k = \sqrt{k_1^2 + k_2^2}$.

The linear stability analysis may give criteria for predicting the cell size of cellular detonations. One may ask whether the wavenumber corresponding to the maximum growth rate, regardless of the mode number, gives the correct cell spacing. For the idealized detonation this wavenumber is usually $O(1)$ (Short & Stewart 1998; Sharpe 1997*a*; Short 1997) which would predict a cell size of about the order of the steady detonation induction zone length. However, although such small cells are seen in the early stages of the cellular instability, experiments show that the final cell size is between one and two orders of magnitude greater than the corresponding steady induction zone length (Lee 1984). Short & Stewart (1997, 1998) suggest that an alternative criterion for predicting the cell spacing is given by the wavenumber corresponding to the largest group speed, $c_g = \partial \mathrm{Im}(\sigma)/\partial k$, of the fundamental mode, which occurs at much smaller wavenumbers for the idealized detonation. For a detonation in a tube of width W one would expect the cell size to be based on the wavenumber with the maximum growth rate or group speed compatible with the tube width, i.e. such that $k = 2\pi n/W$, $n = 0, 1, 2, \ldots$ (Bourlioux & Majda 1992).

Figure 13(*a,b*) shows the variation of the eigenvalues and group speeds with wavenumber for the pathological detonation when $E_1 = 35$, $E_2 = 50$. For one-dimensional disturbances, $k = 0$, the fundamental mode and first overtone are unstable, with eigenvalues $\sigma = 0.0565 + 0.0664\mathrm{i}$ and $\sigma = 0.0177 + 0.7780\mathrm{i}$ respectively. The higher-frequency modes are all stable to one-dimensional perturbations. As the wavenumber increases the growth rate and frequency of the fundamental mode also increase, until the growth rate reaches a maximum of 0.1577 at $k = 1.03$, which is also the largest overall growth rate. The growth rate then decreases as the wavenumber is increased further, until the mode becomes stable to wavenumbers above $k = 2.80$. Similarly, the growth rate of the first overtone also initially increases as k is increased from zero, until it reaches a maximum of 0.1241 at $k = 2.59$. This mode is stable to wavenumbers above $k = 4.83$. Meanwhile, the second overtone becomes unstable at $k = 3.15$, reaches a maximum of 0.0427 before becoming stable again at $k = 5.53$. The third and higher overtones lie entirely within the stable region $\mathrm{Re}(\sigma) < 0$ for all wavenumbers, so that the detonation is stable to wavenumbers above $k = 5.53$.

Figure 13(*c,d*) shows the variation of the phase speeds, $c_p = \mathrm{Im}(\sigma)/k$, and group speeds, $c_g = \partial \mathrm{Im}(\sigma)/\partial k$ of the unstable modes with wavenumber. The group speed of the fundamental mode increases sharply as the wavenumber increases from zero and has a maximum of $c_g = 0.295$ at $k = 0.13$, and the group speed decreases as

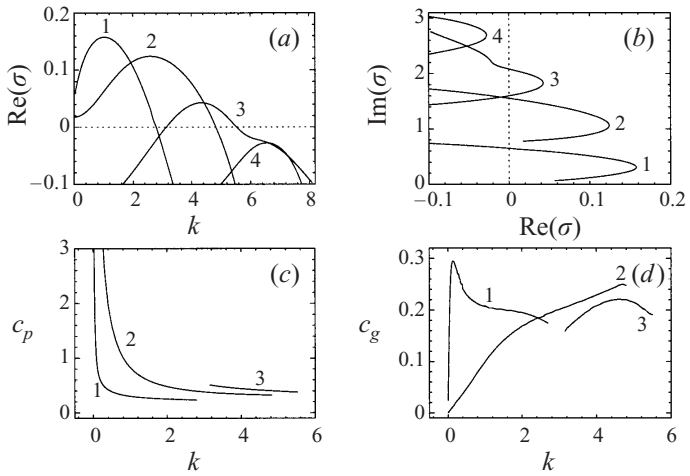

FIGURE 13. Variation of the eigenvalues, phase speeds and group speeds of the modes with wavenumber for the pathological detonation with $E_1 = 35$, $E_2 = 50$, $Q_1 = 100$, $Q_2 = -75$, $\alpha = 1$, $\gamma = 1.2$. (*a*) Growth rates versus wavenumber, (*b*) frequencies versus growth rates, (*c*) phase speeds of unstable modes versus wavenumber, and (*d*) group speeds of unstable modes versus wavenumber. The modes are numbered in order of ascending frequency.

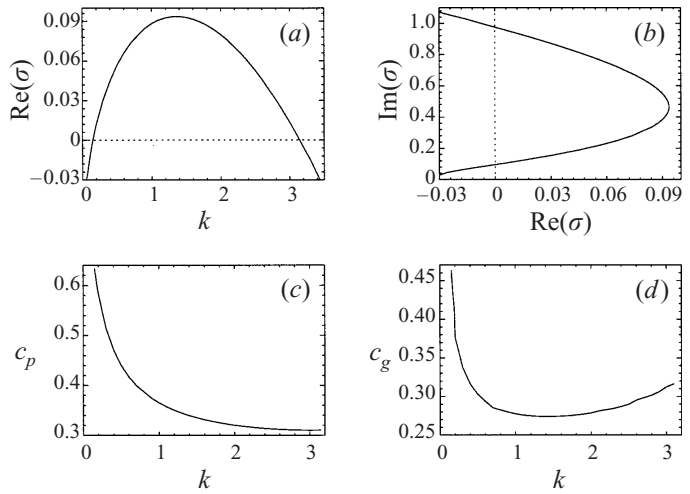

FIGURE 14. Variation of the eigenvalue, phase speed and group speed of the fundamental mode with wavenumber for the pathological detonation with $E_1 = 20$, $E_2 = 50$, $Q_1 = 100$, $Q_2 = -75$, $\alpha = 1$, $\gamma = 1.2$. (*a*) Growth rates versus wavenumber, (*b*) frequency versus growth rates, (*c*) unstable phase speed versus wavenumber, and (*d*) unstable group speed versus wavenumber.

the wavenumber is increased further. The group speed of the first overtone, however, increases monotonically with the wavenumber and has a maximum of $c_g = 0.250$ near the neutrally stable wavenumber $k = 5.53$. Lastly, the group speed of the second overtone increases from its value at the lower neutrally stable wavenumber $k = 3.15$, reaches a maximum of $c_g = 0.221$ at $k = 4.60$ before decreasing again. Therefore a cell spacing based on the highest group speed would be given by the maximum of the fundamental mode at $k = 0.13$, i.e. a wavelength of 48.3 steady induction zone

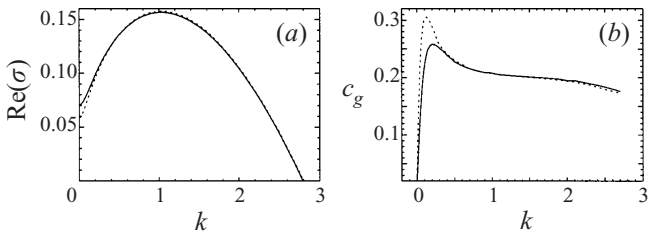

FIGURE 15. (*a*) Variation of the growth rates with wavenumber, (*b*) variation of the group speeds with wavenumber for the fundamental mode for overdriven detonations with $f - f^p = 5 \times 10^{-5}$ (dotted line) and $f - f^p = 0.02$ (solid line). $E_1 = 35$, $E_2 = 50$, $Q_1 = 100$, $Q_2 = -75$, $\alpha = 1$, $\gamma = 1.2$.

lengths, compared to $k = 1.03$, i.e. a wavelength of 6.10 steady induction zone lengths, based on the largest overall growth rate.

Figure 14 shows the variation of the eigenvalues, phase speed and group speed with wavenumber for $E_1 = 20$, $E_2 = 50$. In this case the pathological detonation is stable to one-dimensional disturbances. The fundamental mode remains stable to disturbances with wavenumbers less than $k = 0.15$. It becomes neutrally stable at $k = 0.15$, the growth rate increases to a maximum of 0.0936 at $k = 1.36$ and then decreases until it becomes stable again above wavenumbers of $k = 3.14$. The higher-frequency modes are now stable for all wavenumbers, so that only the fundamental mode is unstable. The group speed is now a maximum, $c_g = 0.463$, at the lower neutrally stable wavenumber, $k = 0.15$. Hence a cell size based on the maximum growth rate is 4.61 steady induction zone lengths, while that based on maximum group speed is 41.9 steady induction zone lengths.

The above response of the pathological detonation to multi-dimensional perturbations, where, for given a given parameter set, there is a critical mode number above which modes are stable to all wavenumbers, and where, as the detonation becomes more stable the fundamental mode remains unstable to a range of wavenumbers, but the higher frequency modes all become stable, is qualitatively similar to the idealized CJ detonation.

7.2. *Overdriven detonations*

We now investigate whether the sensitivity to the degree of overdrive near the pathological degree of overdrive seen for one-dimensional disturbances also occurs for multi-dimensional disturbances. Figure 15 shows the dependence of the growth rate and group velocity on wavenumber for two overdriven detonations with $f - f_p = 5 \times 10^{-5}$ and $f - f_p = 0.02$, when $E_1 = 35$, $E_2 = 50$. On the scale of figure 15(*a*), the growth rates are virtually indistinguishable except at low wavenumbers. Indeed, both detonations have a maximum growth rate at $k = 1.03$, the same wavenumber as for the pathological detonation. However, there is a large difference in the group speeds at low wavenumbers. For $f - f^p = 5 \times 10^{-5}$, the maximum group speed is $c_g = 0.305$ at $k = 0.12$ and for $f - f^p = 0.02$ the maximum is 0.258 at $k = 0.23$, compared with a maximum of 0.295 at $k = 0.13$ for the pathological detonation. The predicted cell wavelengths are thus 48.3, 52.4 and 27.3 steady induction zone lengths for detonations with $f = f^p$, $f - f^p = 5 \times 10^{-5}$ and $f - f_p = 0.02$, respectively. Hence in this case a cell size based on the wavenumber with the largest group speed is very sensitive to the degree of overdrive near $f = f^p$, whereas the criterion based on the wavenumber with the highest growth rate is not at all sensitive.

8. Conclusions

Using a normal mode approach, we have investigated the linear stability of pathological detonations for a model system. We have shown that the response of the pathological detonation to both one- and two-dimensional disturbances is very similar to that of CJ detonations, apart from the existence of stable modes which formally do not exist for CJ and overdriven detonations of infinite length.

We have also shown that even though the boundedness condition for the pathological and overdriven detonations are applied at very different singular points, the linear spectrum is not singular as $f \to f^p$. This presumably means that the solution of the linearized equations that is unbounded at the pathological point is the same solution as the one that is unbounded at the equilibrium point.

For overdriven detonations, the migration of the one-dimensional modes as the degree of overdrive is increased is very sensitive to changes in f near the pathological speed, and oscillatory modes spiral out from their pathological values. Overdriven detonations may be unstable to one-dimensional perturbations even when the unsupported pathological detonation is stable. For multi-dimensional disturbances the group speed is also sensitive to the degree of overdrive at low wavenumbers. Thus a cell size based on the wavenumber with the highest group speed is itself sensitive to the degree of overdrive, whereas one based on maximum growth rate is not. Note, however that using the group speed criterion seems to give better agreement with the cells sizes found in experiment (Lee 1984). This suggests that one should take care in drawing conclusions about pathological detonations from numerical simulations with even slightly overdriven detonations.

For the pathological detonation, the boundedness condition on the linearized equations is applied at the pathological point, so that it does not take into account the structure after the pathological point, i.e. the linear stability of the pathological detonation does not depend on whether the detonation is supported or unsupported. However, since the structures of the supported and unsupported steady pathological detonation are quite different, the long-time nonlinear stability of the two waves might also be very different, especially for very unstable detonations. For instance, once the detonation is in the unstable regime, the single sonic point of the supported wave can easily be destroyed, so that disturbances from downstream of the detonation can reach the front, whereas the supersonic branch of the unsupported wave would be much more difficult to destroy.

In a sequel (Sharpe & Falle 1999) we intend to perform both one- and two-dimensional numerical simulations of pathological detonations in order to compare with the linear stability analysis and to investigate the nonlinear behaviour of the instability for both supported and unsupported detonations. Such simulations require efficient, adaptive codes, such as that developed by Falle & Giddings (1993), which we intend to use for this purpose.

The author acknowledges support from PPARC during the course of this work. I would also like to thank S. A. E. G. Falle for careful reading of the manuscript and suggestions for improvement.

REFERENCES

Bourlioux, A. & Majda, A. J. 1992 Theoretical and numerical structure for unstable two-dimensional detonations. *Combust. Flame* **90**, 211–229.

Bourlioux, A., Majda, A. J. & Roytburd, V. 1991 Theoretical and numerical structure for unstable one-dimensional detonations. *SIAM J. Appl. Maths* **51**, 303–343.

Erpenbeck, J. J. 1962 Stability of steady-state equilibrium detonations. *Phys. Fluids* **5**, 604–614.

Erpenbeck, J. J. 1964 Stability of idealized one-reaction detonations. *Phys. Fluids* **7**, 684–696.

Erpenbeck, J. J. 1966 Detonation stability for disturbances of small transverse wavelength. *Phys. Fluids* **9**, 1203–1306.

Falle, S. A. E. G. & Giddings, J. R. 1993 Body Capturing. In *Numerical Methods for Fluid Dynamics 4* (ed. K. W. Morton & M. J. Baines), pp. 337–343. Clarendon.

Fickett, W. & Davis, W. C. 1979 *Detonation*. Berkeley: University of California Press.

Fickett, W. & Wood, W. W. 1966 Flow calculations for pulsating one-dimensional detonations. *Phys. Fluids* **9**, 903–916.

Khokhlov, A. M. 1989 The structure of detonation waves in supernovae. *Mon. Not. R. Astron. Soc.* **239**, 785–808.

Kriminski, S. A., Bychkov, V. V. & Liberman, M. A. 1998 On the stability of thermonuclear detonation in supernovae events. *New Astron.* **3**, 363–377.

Landau, L. D. & Lifshitz, E. M. 1959 *Fluid Mechanics*. Permagon.

Lee, H. I. & Stewart, D. S. 1990 Calculation of linear detonation stability: one-dimensional instability of plane detonation. *J. Fluid Mech.* **216**, 103–132.

Lee, J. H. S. 1984 Dynamic parameters of gaseous detonations. *Ann. Rev. Fluid Mech.* **16**, 311–336.

Neumann, J. Von 1942 In *John von Neumann, Collected Works* (ed. A. H. Taub), vol. 6, ch. 20, pp. 203–218. Pergamon.

Sharpe, G. J. 1997*a* Linear stability of idealized detonations. *Proc. R. Soc. Lond.* A **453**, 2603–2625.

Sharpe, G. J. 1997*b* Detonation waves in type I supernovae. PhD thesis, University of Leeds.

Sharpe, G. J. & Falle, S. A. E. G. 1998 One-dimensional numerical simulations of idealized detonations. *Proc. R. Soc. Lond.* A, **455**, 1203–1223.

Sharpe, G. J. & Falle, S. A. E. G. 1999 One-dimensional nonlinear stability of pathological detonations. *J. Fluid Mech.* (Submitted).

Short, M. 1996*a* A parabolic linear evolution equation for cellular detonation instability. *Combust. Theory Modelling* **1**, 313–346.

Short, M. 1996*b* An asymptotic derivation of the linear stability of the square-wave detonation using the Newtonian limit. *Proc. R. Soc. Lond.* A **452**, 2203–2224.

Short, M. 1997 Multidimensional linear stability of a detonation wave at high activation energy. *SIAM J. Appl. Maths* **57**, 307–326.

Short, M. & Quirk, J. J. 1997 On the nonlinear stability and detonability of a detonation wave for a model three-step chain-branching reaction. *J. Fluid. Mech.* **339**, 89–119.

Short, M. & Stewart, D. S. 1997 Low-frequency two-dimensional instability of plane detonation. *J. Fluid Mech.* **340**, 249–295.

Short, M. & Stewart, D. S. 1998 Cellular detonation stability - I: A normal-mode linear analysis. *J. Fluid Mech.* **368**, 229–262.

Short, M. & Stewart, D. S. 1999 The multi-dimensional stability of weak heat release detonations. *J. Fluid Mech.* **382**, 109–135.

Wasow, W. 1965 *Asymptotic Expansions for Ordinary Differential Equations*. Interscience.

Wiggins, D. J. R., Sharpe, G. J. & Falle, S. A. E. G. 1998 Double detonations at the core-envelope boundary in type Ia supernovae. *Mon. Not. R. Astron. Soc.* **301**, 405–413.

Williams, D. N., Bauwens, L. & Oran, E. S. 1996 A numerical study of the mechanisms of self-reignition in low-overdrive detonations. *Shock Waves* **6**, 93–110.

Wood, W. W. & Salsburg, Z. W. 1960 Analysis of steady-state supported one-dimensional detonations and shocks. *Phys. Fluids* **4**, 549–566.